JPET Fast Forward. Published on May 8, 2017 as DOI: 10.1124/jpet.117.241679
This article has not been copyedited and formatted. The final version may differ from this version.

XE991 and Linopirdine are state-dependent inhibitors for Kv7/KCNQ channels that favor activated single subunits

Derek L Greene, Seungwoo Kang, and Naoto Hoshi

Department of Pharmacology (DLG, SK, NH), Department of Physiology and Biophysics (NH), University of California, Irvine 360 Med Surge II, Irvine CA 92697, USA

Current address for SK. Department of Anesthesiology, Pharmacology and Physiology, Rutgers, The State University of New Jersey, New Jersey Medical School, 185 South Orange Avenue, Newark, NJ, USA.

Running Title Page

Running title: XE991 as an activated-subunit inhibitor

Corresponding author: Naoto Hoshi,

Address: Department of Pharmacology, University of California, Irvine, 360 Med Surge II, Irvine CA 92697, USA 92697, USA

Tel: +1-(949)-824-0969

Fax: +1-(949)-824-4855

e-mail: nhoshi@uci.edu

Number of Text pages, 14 pages

Number of tables, 0

Number of Figures, 8

Number of references, 28

Number of words in the Abstract, 235

Number of words in the introduction, 359

Number of words in the discussion, 462

List of Abbreviations: CHO, Chinese hamster ovary; mCit, monomeric citrine; TIRF, total internal reflection florescence; k_{on}, association rate constant; k_{off}, dissociation rate constant; Kd, inhibition constant; τ, time constant.

Recommended section, Cellular and Molecular Pharmacology

JPET Fast Forward. Published on May 8, 2017 as DOI: 10.1124/jpet.117.241679
This article has not been copyedited and formatted. The final version may differ from this version.

Abstract

M-channel inhibitors, especially XE991, are increasingly being used in animal experiments. However, insufficient characterization of XE991 at times confounds the interpretation of results when using this compound. Here, we demonstrate that XE991 and linopirdine are state-dependent inhibitors that favor the activated-subunit of neuronal Kv7/KCNQ channels. We performed patch clamp experiments on homomeric Kv7.2 or heteromeric Kv7.2/3 channels expressed in Chinese hamster ovary cells in order to characterize XE991 and linopirdine. Both inhibitors were not efficacious around the resting membrane potential of cells in physiological conditions. Inhibition of Kv7.2 and Kv7.2/3 channels by XE991 was closely related with channel activation. When voltage dependence of activation was left-shifted by retigabine or right-shifted by the mutation, Kv7.2(R214D), the shift in half activation voltage proportionally coincided with the shift in the half-effective potential for XE991 inhibition. Inhibition kinetics during XE991 wash-in were facilitated at depolarized potentials. Ten-minute washout of XE991 resulted in ~30% current recovery, most of which was attributed to surface transport of Kv7.2 channels. Linopirdine also exhibited similar inhibition characteristics with the exception of near complete current recovery after washout at depolarized potentials. Inhibition kinetics of both XE991 and linopirdine were not as sensitive to changes in voltage as would be predicted by open channel inhibition. Instead, they were well explained by binding to a single activated subunit. The characteristics of XE991 and linopirdine should be taken into account when these M-channel inhibitors are used in experiments.

Introduction

Subclasses of Kv7/KCNQ subunits form tetrameric channels that underlie the M-current, a low threshold non-inactivating voltage-gated potassium current, which regulates neuronal excitability (Delmas and Brown, 2005; Greene and Hoshi, 2017; Jentsch, 2000). Activation of Gq-coupled receptors such as muscarinic acetylcholine receptors (m1 and m3) suppresses the M-current and induces transient hyperexcitability in a wide range of neurons (Delmas and Brown, 2005). Accordingly, M-channel inhibitors were developed in hopes of ameliorating defective neuronal activity such as in Alzheimer's dementia. Linopirdine is one such prototypical compound that was found to have a cognitive enhancing effect in an animal model (Fontana et al., 1994). However, linopirdine did not pass phase 3 clinical trials (Rockwood et al., 1997). XE991 was developed as an improved compound with a similar chemical structure (Zaczek et al., 1998). Although no clinical trials have been conducted for this compound, XE991 has increasingly been used in cell culture and animal experiments to investigate physiological (Martinello et al., 2015; Vetter et al., 2013; Young and Thomas, 2014) and pathological roles (Kay et al., 2015; Mani et al., 2013) of the M-current.

It has been shown that KCNQ2 gene knockout is lethal (Soh et al., 2014; Watanabe et al., 2000). However, administration of linopirdine is well tolerated in humans (Pieniaszek et al., 1995; Rockwood et al., 1997), as well as animals for linopirdine and XE991 (Fontana et al., 1994; Zaczek et al., 1998). In addition, even though XE991 is a highly potent inhibitor, it sometimes requires prolonged incubation to inhibit (Yue and Yaari, 2004), or may have no observed effect (Romero et al., 2004). These lines of evidence suggest that there are conditions where these Kv7 channel inhibitors are not efficacious.

Since XE991 is among the predominant choices for inhibiting Kv7 channels, inconsistencies in the literature denote a need to further characterize its mode of inhibition. To this end we performed an electrophysiological study in a heterologous expression system. We determined the conditions where these compounds are efficacious, as well as their mode of interaction and addressed the past inconsistencies regarding the washout of these compounds. The determined characteristics of XE991 and linopirdine should be pertinent for experimenters utilizing these inhibitors.

Materials and Methods

Reagents and Plasmids. Linopirdine (1,3-Dihydro-1-phenyl-3,3-bis(4-pyridinylmethyl)-2H-indol-2-one dihydrochloride), XE991 dihydrochloride (10,10-bis(4-Pyridinylmethyl)-9(10H)-anthracenone dihydrochloride), and Exo1 (2-[(4-Fluorobenzoyl)amino]-benzoic acid methyl ester) were purchased from Tocris (Bristol, UK). Retigabine (Ethyl N-[2-amino-4-[(4-fluorophenyl)methylamino]phenyl]carbamate) was purchased from Alomone Labs (Jerusalem, Israel). Concanavalin A was purchased from Sigma-Aldrich (St. Louis, MO, USA). Mammalian expression plasmids containing rat Kv7.2, Kv7.3 (Hoshi et al., 2003) and Kv7.2-mCit (Kosenko et al., 2012) have been described. Kv7.2 mutation (R214D) was generated using QuickChange II XL site-directed mutagenesis (Agilent Technologies, San Diego, CA, USA), and was validated by DNA sequencing.

Cell Culture. Chinese hamster ovary hm1 cells (Jiang et al., 2015) were cultured in α minimum essential media containing 5% fetal calf serum and 500 μg/ml G418 sulfate. Cells were maintained in a humidified incubator at 37 °C with 5% CO_2. CHO cells were grown to 30% confluence on 35 mm plates before being transfected with 1 μg plasmid DNA and 4 μl LT1 reagent (Mirus Bio LLC, Madison, WI, USA).

Electrophysiology. All patch clamp recordings were performed at room temperature on isolated CHO cells using an Axon Multiclamp 700B patch clamp amplifier (Molecular Devices). Data were acquired using pClamp software (version 10; Molecular Devices). Signals for current traces with ≤1 second duration were sampled at 2 kHz and low pass-filtered at 1 kHz. Current recordings between 1-15 seconds were sampled at 500 Hz and those longer than 15 seconds was sampled at 250 Hz. Whole cell patch clamp recordings on CHO hm1 cells has been described

JPET Fast Forward. Published on May 8, 2017 as DOI: 10.1124/jpet.117.241679
This article has not been copyedited and formatted. The final version may differ from this version.

previously (Kosenko et al., 2012). Briefly, cells were constantly perfused with Q2 solution containing 144 mM NaCl, 5 mM KCl, 2 mM $CaCl_2$, 0.5 mM $MgCl_2$, 10 mM glucose, and 10 mM HEPES (pH 7.4). Patch pipettes (3–4 MΩ) were filled with intracellular solution containing 135 mM potassium aspartate, 2 mM $MgCl_2$, 3 mM EGTA, 1 mM $CaCl_2$, 4 mM ATP, 0.1 mM GTP, 10 mM HEPES (pH 7.2). Successful patches that maintained Rs <6 MΩ were selected for experiments. Liquid junction potential was not corrected in this study.

Live Cell Imaging. Protocol for TIRF-based assessment of surface transport of Kv7.2 channel has been described previously (Jiang et al., 2015). Briefly, one day after transfection cells were replated onto 18 mm round cover-glasses. On the second day after transfection, cells were used for TIRF experiments. For recording, medium was replaced with Q2 solution. For Exo1 experiments, cells were pretreated with 100 μM Exo1 in Q2 solution at room temperature for 2 minutes prior to proceeding with experiments. Fluorescence emission was acquired using an inverted microscope IX-81 (Olympus Tokyo, Tokyo, Japan) with an ImageEM CCD camera (Hamamatsu Photonics, Hamamatsu, Shizuoka Japan) controlled by MetaMorph 7.6.3 (Molecular Devices, Sunnyvale, CA, USA). For excitation in TIRF experiments, a 515 nm diode-pumped solid-state laser (Cobolt, Stockholm, Sweden) with an acousto-optic tunable filter was used with a TIRF module (Olympus). Emission images were obtained through a dual-view module (Photometrics, Tucson, AZ, USA) with ET535/30m, ET480/40m emission filters and a T505lpxr dichroic mirror (Chroma Technology, Bellows Falls, VT, USA). 100 ms exposure time of images was taken every 10 seconds for time-lapse imaging measurements.

Statistics. The activation curves were obtained by non-linear regression to a Boltzmann equation, $Y = (1+\exp((V_{1/2}-x)/k))^{-1}$ where x is membrane potential, $V_{1/2}$ is the half activation potential, and k is the slope factor unless stated otherwise in the text. All results are expressed as

the mean ± s.e.m. Statistical significance of the results was assessed by non-parametric ANOVA (Kruskal-Wallis test) followed by Dunn's multiple comparisons test or Mann-Whitney test. All statistical tests were performed by a computer program Prism 6 (GraphPad, La Jolla, CA, USA). $P < 0.05$ is considered significant.

Results

Voltage-dependence of XE991 inhibition is closely related to activation of Kv7 channels rather than the membrane potential per se.

During our previous study (Kay et al., 2015), we observed that XE991 is more effective in highly active neurons compared to less active neurons. It has previously been reported that M-current inhibition by XE991 is voltage dependent and that under some conditions it does not inhibit the M-current (Romero et al., 2004). We alternatively reasoned that these characteristics of XE991 are derived from state-dependent inhibition rather than voltage-dependent inhibition since the activation threshold of Kv7 channel is very close to the resting membrane potential.

We characterized the voltage dependency of homomeric Kv7.2 and heteromeric Kv7.2/3 channel activation to XE991-mediated inhibition. Exposure to 10 μM XE991 for 25 seconds had no effects when cells were held at -70 mV (Fig. 1A), while showing near complete inhibition when XE991 was applied at potentials more positive than -30 mV (Fig. 1B). XE991-mediated inhibition of Kv7.2 or Kv7.2/3 channels showed voltage-dependence with half-inhibition potentials of -51.6 ± 0.0 mV for Kv7.2 channels, and -50.7 ± 0.9 mV for Kv7.2/3 channels (Fig. 1C & D). When XE991-mediated inhibition is plotted against relative activation of Kv7.2 and Kv7.2/3 channels (Fig. 1E), it indicates that XE991 is only effective when cells are held at potentials where Kv7 channels are activated more than 1%.

To further characterize relationships between channel activation and XE991 mediated inhibition, we shifted the activation voltage of Kv7 channels to more hyperpolarized potentials with retigabine and evaluated whether it changed the efficacy of XE991 (Fig. 2). In the presence of 10 μM retigabine, the half-activation voltage of Kv7.2 was -47.0 ± 0.8, a -24 mV shift from the

control (Fig. 2B). The half-inhibition potential of XE991 also shifted -24 mV from the control (-75.2 ± 0.6 mV, n = 5, Fig. 2B & C). Notably, XE991 inhibited Kv7.2 current at a holding potential of -70 mV in the presence of retigabine (Fig. 2A), a potential at which XE991 did not inhibit Kv7.2 current in control and close to the resting membrane potential in neurons (Fig. 1C).

An additional characterization of voltage-dependent inhibition by XE991 was assessed in a mutant Kv7.2 channel (R214D), which had a 26 mV right-shift in the activation potential (3.4 ± 14.0 mV, Fig. 3). Accordingly, the rightward shift in the voltage-dependence of activation coincided with an equivalent rightward shift (26 mV) in the half-inhibition potential (-26.3 ± 0.27 mV, Fig. 3B). Relationships between inhibition by XE991 and channel activation was maintained in this condition (Fig. 3C). Interestingly, the voltage dependence of Kv7 channel activation vs. inhibition by XE991 followed a linear function with a slope of 0.97 ± 0.03, when comparing wild-type, retigabine-treated and Kv7.2(R214D) channels (Fig. 3D), suggesting a close relation between voltage-dependence of Kv7.2 channel activation and efficacy of XE991.

Inhibition Kinetics of XE991

We then tested the effect of membrane potential on inhibition kinetics (Fig. 4). First, cells were held at -70 mV, a potential where XE991 has no effect, followed by a 20 second depolarization to various test potentials with or without XE991 and then analyzed the time course of inhibition. XE991 inhibited Kv7.2 currents with time constants that decreased with increasing depolarization (Fig. 4A–C). An interesting question would be whether such differences in inhibition kinetics change the potency of XE991 or only the speed of inhibition. To address this question, we measured the time course of Kv7.2 current inhibition by 1 μM XE991, which is close to the reported IC_{50} of XE991 (Wang et al., 1998), using test pulses with 20-s interval at holding potentials of either 0 mV or -40 mV (Fig. 4D). Even though there was a difference in the

JPET Fast Forward. Published on May 8, 2017 as DOI: 10.1124/jpet.117.241679
This article has not been copyedited and formatted. The final version may differ from this version.

speed of current inhibition depending on holding potentials, both conditions reached almost complete block after 5 min.

Limited recovery of Kv7 current after washout of XE991 is predominantly due to channel trafficking.

There are conflicting reports regarding recovery of Kv7 currents from XE991 after washout. Some groups considered inhibition by XE991 to be reversible (Rennie et al., 2001; Yue and Yaari, 2004; Zaika et al., 2006), while others considered it irreversible (Brueggemann et al., 2012; Wladyka and Kunze, 2006). To test this, we first treated CHO cells expressing Kv7.2 channels with 10 μM XE991 at 0 mV for 25 seconds, and then held cells at holding potentials of either -70 or -30 mV during the wash process to assess current recovery (Fig. 5). Washout experiments between these two potential did not show significant difference (20.2 ± 3.9% and 18.2 ± 2.9% recovery after 10 minute washout at -70 mV and -30 mV holding potential respectively, Fig. 5A & B). Control experiments without XE991 showed stable Kv7.2 current in this recording condition (Fig. 5B). We then measured rate of current recovery from distinct concentrations of XE991 (0.25, 1, 10 μM), which also showed no differences (Fig. 5C). These results suggest that current recovery after washout is very limited for XE991. We then tested heteromeric Kv7.2/3 channels, which showed similar slow and limited recovery after washout [33.4 ± 5.9% (n = 6) recovery at -70 mV, 37.8 ± 3.8% (n = 6) at -30 mV after 10 minute wash].

30% turnover of Kv7.2 channel in 10 minutes is comparable to surface transport of Kv7.2 subunit that we described previously in CHO cells (Jiang et al., 2015). To evaluate the contribution of Kv7.2 channel trafficking to the current recovery, we tested whether an exocytosis inhibitor, 100 μM Exo1 (Feng et al., 2003), can suppress current recovery after washout. We first confirmed the effects of 100 μM Exo1 on surface transport of Kv7.2 channel

by total internal reflection fluorescence (TIRF) measurements using monomeric citrine-tagged Kv7.2 channel, Kv7.2-mCit. TIRF selectively illuminates <100 nm from the cover glass, which can be used to monitor Kv7.2 surface transport at the bottom surface of cells (Jiang et al., 2015). To confirm Exo1 ability to suppress exocytosis, we inhibited endocytosis by 50 μg/mL concanavalin A, which induced a gradual increase of TIRF signal of Kv7.2-mCit due to constitutive exocytosis (Fig. 5D) (Jiang et al., 2015). 2 minute pretreatment with 100 μM Exo1 resulted in a 75 ± 5% reduction in concanavalin A-induced increase in TIRF signals from Kv7.2-mCit (Fig. 5D), confirming that the majority of exocytosis is inhibited in this condition. Using this condition, we examined whether Exo1 prevents recovery of Kv7.2 current after 10 μM XE991 washout. 100 μM Exo1 application alone did not inhibit Kv7.2 current (0.98 $\pm$ 0.06, n = 6). In the control washout without Exo1, Kv7.2 current recovered 32.3 $\pm$ 2.1% after 10 min washout at a holding potential of -70 mV (Fig. 5E). In the presence of 100 μM Exo1, current recovery was reduced to 12.1 ± 2.1% (Fig. 5E & F). To further assess whether open probability of Kv7.2 affects current recovery, we tested washout in the presence of 10 μM retigabine at -30 mV as well as washout at a holding potential of 0 mV. These conditions did not alter current recovery (Fig. 5F). We concluded that current recovery after washout of XE991 is mostly derived from new Kv7 channels surfaced to the plasma membrane rather than dissociation of XE991 from Kv7.2 channel.

Linopirdine shares basic features with XE991.

Since current recovery after washout of XE991 did not accurately reflect dissociation of XE991, we examined linopirdine to evaluate inhibition kinetics of this type of Kv7 channel inhibitor. Linopirdine is a prototypical M-channel inhibitor that was developed prior to and considered to be structurally similar to XE991 (Zaczek et al., 1998). As summarized in Fig. 6, 30 μM

JPET Fast Forward. Published on May 8, 2017 as DOI: 10.1124/jpet.117.241679
This article has not been copyedited and formatted. The final version may differ from this version.

linopirdine showed voltage-dependent inhibition of Kv7.2 current with a half-inhibition potential at -55.7 ± 0.4 mV (Fig. 6A & B), which is very close to that of XE991. We then assessed inhibition kinetics of linopirdine (30 μM) at various test potentials using the same voltage protocols as used in XE991 (Fig. 6D – F). Similar to XE991, inhibition time constants of linopirdine were decreased with more depolarized potentials (Fig. 6F).

Although wash-in inhibition was very similar to XE991, there was a difference in current recovery during washout. When linopirdine-treated CHO cells were washed at a holding potential of -70 mV, Kv7.2 currents showed 24.2 ± 4% recovery after 10 minutes (n = 6) (Fig. 7A & B), comparable to that of XE991. However, when cells were held at -30 mV, Kv7.2 currents showed almost full recovery after 10 minute wash (93.4 ± 4.2%, n = 5, Fig. 7A & B). Similar recovery profile was observed with heteromeric Kv7.2/3 channels (Fig. 7C). To further characterize current recovery at depolarized potentials, Kv7.2 current was monitored by 500-ms hyperpolarized steps with 20-s interval. Time courses of current recovery (Fig. 7D) were best fit by a single exponential function with time constants as summarized in Fig. 7E, which was facilitated as holding potentials were depolarized (Fig. 7D & E).

Quantitative model for XE991 and linopirdine.

Our results so far suggest that inhibition kinetics of XE991 and linopirdine were closely related with the activation state of Kv7.2 channel. A common mechanism of state-dependent ion channel inhibitors is open channel inhibition. Therefore, we first assessed this mechanism. If XE991 and linopirdine interact with the channel at the open state, then wash-in and washout time constants should show close correlation with channel activation. Namely, if inhibitors interact only with open channels, then the rate of association at the half activation potential for Kv7.2 channel (-21

mV, Fig. 8) should be nearly twice that of the rate constant at maximal activation since duration of single channel opening at $V_{1/2}$ is a half of that at maximal activation.

We assumed a single step binding reaction for XE991 or linopirdine (inhibitors, INH), which can be described as

$$\text{Kv7.2} + \text{INH} \underset{k_{off}}{\overset{k_{on}}{\rightleftharpoons}} \text{Kv7.2:INH}$$

where k_{on} ($M^{-1}s^{-1}$) is the second-order association rate constant and k_{off} (s^{-1}) is the first-order dissociation rate constant. Thus, this reaction can be described as

$$\tau_{in}^{-1} = k_{on}[\text{INH}] + k_{off} \quad (1)$$

$$\tau_{rec}^{-1} = k_{off} \quad (2)$$

using the inhibition time constant (τ_{in}) and concentration of inhibitors, [INH], as described (Goldstein and Miller, 1993; Hille, 2001). In addition, k_{off} can be measured directly from the rate of washout as described in equation 2. As equation 1 predicts, inhibition time constants are proportional to the reciprocal of the rate constant. Thus, we plotted normalized wash-in time constants to reciprocals of the activation curve (Ch_a^{-1}, Fig. 8B). To our surprise, neither wash-in nor washout time constants overlapped with Ch_a^{-1} (Fig. 8B & C). Instead, best-fit powers for wash-in were 0.19 ± 0.06 for linopirdine, 0.26 ± 0.03 for XE991, which were close to one-fourth power of the activation curve (Fig. 8B, $Ch_a^{1/4}$). A similar trend was observed for washout of linopirdine (0.36 ± 0.006 for linopirdine washout, Fig. 8C). We did not perform this analysis for XE991 washout since it was not voltage-dependent. Considering a single channel is composed of four subunits, a best fit to the one-fourth power of channel activation suggests binding interactions are more related to activation of a single subunit. To evaluate this, we estimated

single subunit activation by applying the fourth power Boltzmann equation to Kv7.2 channel activation:

$$Y = (1+\exp((V_{1/2}-x)/k))^{-4} \quad (3)$$

where x is the membrane potential, $V_{1/2}$ is the half activation potential of a single subunit, and k is the slope factor. Best-fit curve for channel activation is shown as purple curve in Fig. 8A (Sub_a^4), and red curve shows a derived activation curve for a single subunit (Sub_a). Reciprocals of predicted single subunit activation curves were also in good agreement with the inhibition kinetics of XE991 and linopirdine (Fig. 8B & C, red curve). Furthermore, when we recalculated relationships between half-inhibition potentials of XE991 and half-activation potentials of single subunit of Kv7.2 channel using the results shown in Fig. 3D, it showed equivalent relationships (Supplemental Figure 1).

Discussion

It has been previously reported that efficacy of linopirdine and XE991 is voltage-dependent (Romero et al., 2004). We confirmed similar voltage-dependent inhibition by these inhibitors. On the other hand, we also found that shifts in the half-inhibition potential corresponded with equivalent shifts in the half-activation voltage by retigabine or Kv7.2(R214D), which suggests that such changes in efficacy are derived from conformational changes of Kv7.2 channel subunits, rather than from voltage differences across the plasma membrane. The most common class of state-dependent ion channel inhibitor is open channel inhibitors. Therefore, we first suspected this mechanism. In fact, transient channel activation in the presence of inhibitors, as we demonstrated in Fig. 4 & 7, is a signature profile for open channel inhibition (Zagotta et al.,

1990). However, our inhibition kinetic analysis suggests that these inhibitors bind to a single activated subunit rather than an open channel (Fig. 8B & C).

Although, results from linopirdine mirror the majority of findings from XE991, a key difference was that inhibition by linopirdine was reversible at depolarized potentials. This, together with our finding from voltage-dependent wash-in kinetics, suggests that linopirdine can reversibly interact with Kv7.2 channel when subunits are at the active conformation, but is trapped within Kv7.2 channels when subunits are in the resting conformation after binding (Fig. 8D). Unlike linopirdine, we did not observe full recovery for XE991. Furthermore, the majority of current recovery after XE991 washout was due to new channel insertion to the plasma membrane. These findings suggest that binding of XE991 to Kv7.2 channel is apparently irreversible (Fig. 8E). On the other hand, we would like to emphasize that Kv7.2 current can be restored from XE991-mediated inhibition due to channel trafficking, which explains previous observations (Rennie et al., 2001; Yue and Yaari, 2004; Zaika et al., 2006). Our results suggest ~30% recovery per 10 min, but it may depend on cell types and experimental conditions.

Our findings in this report suggest that XE991 might not be efficacious for cells staying at resting membrane potentials such as in silent or scarcely firing neurons. Co-administration of XE991 and retigabine would be helpful to remove such biased efficacy in animal experiments. For cultured neurons, holding at depolarized potentials during voltage clamp experiments or co-administration of XE991 and retigabine or high potassium would be effective.

Activated subunit inhibition and slow binding kinetics of these inhibitors may explain why these compounds are well tolerated in animals (Kay et al., 2015; Mani et al., 2013; Vetter et al., 2013; Young and Thomas, 2014) without causing lethal seizures, as seen in KCNQ2 gene knockout

mice (Soh et al., 2014; Watanabe et al., 2000). In addition, preferential M-channel inhibition in highly active neurons by these inhibitors would exaggerate neurotransmitter-mediated M-current suppression, which may underlie the cognitive enhancing action of these compounds.

Authorship contribution

Participated in research design: Greene and Hoshi

Conducted experiments: Greene and Hoshi

Contributed new reagents: Kang

Performed data analysis: Greene and Hoshi

Wrote or contributed to the writing of the manuscript: Greene, Kang and Hoshi

References

Brueggemann LI, Kakad PP, Love RB, Solway J, Dowell ML, Cribbs LL and Byron KL (2012) Kv7 potassium channels in airway smooth muscle cells: signal transduction intermediates and pharmacological targets for bronchodilator therapy. *American journal of physiology Lung cellular and molecular physiology* **302**(1): L120-132.

Delmas P and Brown DA (2005) Pathways modulating neural KCNQ/M (Kv7) potassium channels. *Nature reviews Neuroscience* **6**(11): 850-862.

Feng Y, Yu S, Lasell TK, Jadhav AP, Macia E, Chardin P, Melancon P, Roth M, Mitchison T and Kirchhausen T (2003) Exo1: a new chemical inhibitor of the exocytic pathway. *Proceedings of the National Academy of Sciences of the United States of America* **100**(11): 6469-6474.

Fontana DJ, Inouye GT and Johnson RM (1994) Linopirdine (DuP 996) improves performance in several tests of learning and memory by modulation of cholinergic neurotransmission. *Pharmacology, biochemistry, and behavior* **49**(4): 1075-1082.

Goldstein SA and Miller C (1993) Mechanism of charybdotoxin block of a voltage-gated K+ channel. *Biophys J* **65**(4): 1613-1619.

Greene DL and Hoshi N (2017) Modulation of Kv7 channels and excitability in the brain. *Cell Mol Life Sci* **74**(3): 495-508.

Hille B (2001) *Ion channels of excitable membranes*. Sinauer Associates, Inc.

Hoshi N, Zhang JS, Omaki M, Takeuchi T, Yokoyama S, Wanaverbecq N, Langeberg LK, Yoneda Y, Scott JD, Brown DA and Higashida H (2003) AKAP150 signaling complex promotes suppression of the M-current by muscarinic agonists. *Nat Neurosci* **6**(6): 564-571.

Jentsch TJ (2000) Neuronal KCNQ potassium channels: physiology and role in disease. *Nature reviews Neuroscience* **1**(1): 21-30.

Jiang L, Kosenko A, Yu C, Huang L, Li X and Hoshi N (2015) Activation of m1 muscarinic acetylcholine receptor induces surface transport of KCNQ channels through a CRMP-2-mediated pathway. *Journal of cell science* **128**(22): 4235-4245.

Kay HY, Greene DL, Kang S, Kosenko A and Hoshi N (2015) M-current preservation contributes to anticonvulsant effects of valproic acid. *The Journal of clinical investigation* **125**(10): 3904-3914.

Kosenko A, Kang S, Smith IM, Greene DL, Langeberg LK, Scott JD and Hoshi N (2012) Coordinated signal integration at the M-type potassium channel upon muscarinic stimulation. *EMBO J* **31**(14): 3147-3156.

Mani BK, O'Dowd J, Kumar L, Brueggemann LI, Ross M and Byron KL (2013) Vascular KCNQ (Kv7) potassium channels as common signaling intermediates and therapeutic targets in cerebral vasospasm. *Journal of cardiovascular pharmacology* **61**(1): 51-62.

Martinello K, Huang Z, Lujan R, Tran B, Watanabe M, Cooper EC, Brown DA and Shah MM (2015) Cholinergic afferent stimulation induces axonal function plasticity in adult hippocampal granule cells. *Neuron* **85**(2): 346-363.

Pieniaszek HJ, Jr., Fiske WD, Saxton TD, Kim YS, Garner DM, Xilinas M and Martz R (1995) Single-dose pharmacokinetics, safety, and tolerance of linopirdine (DuP 996) in healthy young adults and elderly volunteers. *Journal of clinical pharmacology* **35**(1): 22-30.

Rennie KJ, Weng T and Correia MJ (2001) Effects of KCNQ channel blockers on K(+) currents in vestibular hair cells. *Am J Physiol Cell Physiol* **280**(3): C473-480.

Rockwood K, Beattie BL, Eastwood MR, Feldman H, Mohr E, Pryse-Phillips W and Gauthier S (1997) A randomized, controlled trial of linopirdine in the treatment of Alzheimer's disease. *The Canadian journal of neurological sciences Le journal canadien des sciences neurologiques* **24**(2): 140-145.

Romero M, Reboreda A, Sanchez E and Lamas JA (2004) Newly developed blockers of the M-current do not reduce spike frequency adaptation in cultured mouse sympathetic neurons. *The European journal of neuroscience* **19**(10): 2693-2702.

Soh H, Pant R, LoTurco JJ and Tzingounis AV (2014) Conditional deletions of epilepsy-associated KCNQ2 and KCNQ3 channels from cerebral cortex cause differential effects on neuronal excitability. *The Journal of neuroscience : the official journal of the Society for Neuroscience* **34**(15): 5311-5321.

Vetter I, Hein A, Sattler S, Hessler S, Touska F, Bressan E, Parra A, Hager U, Leffler A, Boukalova S, Nissen M, Lewis RJ, Belmonte C, Alzheimer C, Huth T, Vlachova V, Reeh PW and Zimmermann K (2013) Amplified cold transduction in native nociceptors by M-channel inhibition. *The Journal of neuroscience : the official journal of the Society for Neuroscience* **33**(42): 16627-16641.

Wang HS, Pan Z, Shi W, Brown BS, Wymore RS, Cohen IS, Dixon JE and McKinnon D (1998) KCNQ2 and KCNQ3 potassium channel subunits: molecular correlates of the M-channel. *Science* **282**(5395): 1890-1893.

Watanabe H, Nagata E, Kosakai A, Nakamura M, Yokoyama M, Tanaka K and Sasai H (2000) Disruption of the epilepsy KCNQ2 gene results in neural hyperexcitability. *Journal of neurochemistry* **75**(1): 28-33.

Wladyka CL and Kunze DL (2006) KCNQ/M-currents contribute to the resting membrane potential in rat visceral sensory neurons. *J Physiol* **575**(Pt 1): 175-189.

Young MB and Thomas SA (2014) M1-muscarinic receptors promote fear memory consolidation via phospholipase C and the M-current. *The Journal of neuroscience : the official journal of the Society for Neuroscience* **34**(5): 1570-1578.

Yue C and Yaari Y (2004) KCNQ/M channels control spike afterdepolarization and burst generation in hippocampal neurons. *The Journal of neuroscience : the official journal of the Society for Neuroscience* **24**(19): 4614-4624.

Zaczek R, Chorvat RJ, Saye JA, Pierdomenico ME, Maciag CM, Logue AR, Fisher BN, Rominger DH and Earl RA (1998) Two new potent neurotransmitter release enhancers, 10,10-bis(4-pyridinylmethyl)-9(10H)-anthracenone and 10,10-bis(2-fluoro-4-pyridinylmethyl)-9(10H)-anthracenone: comparison to linopirdine. *The Journal of pharmacology and experimental therapeutics* **285**(2): 724-730.

Zagotta WN, Hoshi T and Aldrich RW (1990) Restoration of inactivation in mutants of Shaker potassium channels by a peptide derived from ShB. *Science* **250**(4980): 568-571.

Zaika O, Lara LS, Gamper N, Hilgemann DW, Jaffe DB and Shapiro MS (2006) Angiotensin II regulates neuronal excitability via phosphatidylinositol 4,5-bisphosphate-dependent modulation of Kv7 (M-type) K+ channels. *The Journal of physiology* **575**(Pt 1): 49-67.

Footnotes

This work was supported by National Institutes of Neurological Disorders and Stroke [Grant R01NS067288] to NH.

Legends for Figures

Figure 1. XE991 inhibits homomeric Kv7.2 and heteromeric Kv7.2/3 channels at more depolarized potential than their activation thresholds. A. Voltage protocol and representative traces showing exposure to 10 μM XE991 at -70 mV for 25 seconds, indicated as black box, was ineffective on Kv7.2 current. Right panel shows expanded traces of indicated time points (1 and 2). **B.** Voltage protocol and representative traces showing 10 μM XE991 completely blocked Kv7.2 current when exposed to XE991 at 0 mV for 25 seconds, indicated as black box. Expanded current traces are also shown. **C.** Summary graph showing voltage–XE991 inhibition relationships and activation curve for homomeric Kv7.2 channels. **D.** Voltage–XE991 inhibition relationships and activation curve for heteromeric Kv7.2/3 channels. **E.** Results shown in panels C and D re-plotted for relative inhibition by XE991 vs. relative activation of channels. Inhibition of XE991 is closely correlated with activation of Kv7 channels in a semi-log plot (Kv7.2: $r = 0.94$, Kv7.2/3: $r = 0.90$). Data shown as average values ± SEM.

Figure 2. Retigabine shifted effective potentials of XE991 to more negative potentials. A. Voltage protocol and representative traces showing when cells were pretreated with 10 μM retigabine, 25 second treatment with 10 μM XE991 (black box) inhibited Kv7.2 current at a holding potential of -70 mV. **B.** Voltage–XE991 inhibition relationships and activation curve for Kv7.2 channels pretreated with 10 μM retigabine. **C.** Activation–XE991 inhibition relationships for Kv7.2 channel from results shown in B. Error bars show SEM.

Figure 3. Kv7.2 mutant (R214D) shifted voltage dependence of activation and XE991 inhibition to more positive potentials. A. Voltage protocol and representative traces showing that 25 second treatment with 10 μM XE991 (black box) inhibited WT Kv7.2 current at a

JPET Fast Forward. Published on May 8, 2017 as DOI: 10.1124/jpet.117.241679
This article has not been copyedited and formatted. The final version may differ from this version.

holding potential of -40 mV while Kv7.2(R214D) mutant channel had minimal inhibition at this holding potential **B.** Voltage–XE991 inhibition relationships and activation curve for Kv7.2(R214D) channels. **C.** Activation–XE991 inhibition relationships for Kv7.2(R214D) channel from results shown in B. **D.** Pooled results for $V_{1/2}$ inhibition and $V_{1/2}$ activation potentials of Kv7.2, retigabine treated Kv7.2 and Kv7.2(R214D) channel. Slope of regression line is also shown. Error bars show SEM.

Figure 4. Voltage-dependence of XE991 inhibition kinetics with Kv7.2 channels. A. Voltage protocol and representative Kv7.2 current traces from 20 second test potential to -40 mV during absence, XE(–), and presence, XE(+), of 10 μM XE991 (red box). Note that in the presence of XE991, the initial activation phase of Kv7.2 current is unaffected. Kv7.2 current ratio of XE(+)/XE(–) showing that current inhibition followed a single exponential decay (lower graph, red line) with the indicated time constant. **B.** Same as A with voltage step to 0 mV. **C.** Inhibition time constants of Kv7.2 current from wash-in experiments at indicated holding potentials measured as shown in A and B. ** < 0.01, non-parametric ANOVA (Kruskal-Wallis test) followed by Mann–Whitney test, n = 6. **D.** Time courses of Kv7.2 current inhibition by 1 μM XE991 at indicated holding potentials. XE991 was applied at t = 0. Cells were held at indicated potentials and current was measured by 500-ms step hyperpolarizations to -60 mV with 20 second intervals. Error bars show SEM.

Figure 5. Kv7.2 current recovery from XE991 washout is limited. A. Representative Kv7.2 current traces showing control, 10 μM XE991 inhibited, and after 10 minute washout at indicated holding potentials. For washout at -30 mV, current was measured by 1-second test potential to -60 mV from a holding potential of -30 mV. For washout at -70 mV, cells were depolarized to 0 mV for 200 ms from a holding potential of -70 mV. **B.** Summary showing slow

and limited recovery of Kv7.2 current after washout in cells held at -30 mV or -70 mV. Wash started at t = 0. **C.** Kv7.2 current recovery from indicated concentrations of XE991 at a holding potential of 0 mV. **D.** TIRF experiments showing 100 μM Exo1 suppressed constitutive exocytosis of mCit tagged Kv7.2 (KCNQ2-mCit) by 50 μg/mL concanavalin A (black box) applied at t = 2 minutes. **E.** Kv7.2 current recovery from 10 μM XE991 at -70 mV showing that 100 μM Exo1 suppressed recovery of the current. Wash started at t = 0. **F.** Summary of current recovery from 10 μM XE991 after10 min washout at indicated conditions. -70 mV wash and -70 mV Exo1 results are from the same data set shown in panel E. ** < 0.01, NS > 0.05, non-parametric ANOVA (Kruskal-Wallis test) followed by Dunn's multiple comparisons test. Error bars show SEM.

Figure 6. Linopirdine replicated most of XE991 effects. A. Voltage protocols and representative Kv7.2 current traces showing voltage-dependent inhibition of 30 μM linopirdine (black box). Right traces show expanded currents from indicated time points 1 and 2. **B.** Pooled results for voltage-inhibition relationships of linopirdine and activation curve for Kv7.2 channels as measured in A. **C.** Results shown in B re-plotted as relative activation against relative inhibition of Kv7.2 by linopirdine. Results of Kv7.2/3 are also included. **D.** Voltage protocol and representative Kv7.2 current traces with a test potential to -40 mV during absence, Lin(–), and presence, Lin(+), of 30 μM linopirdine (red box). Kv7.2 current ratio Lin(+)/Lin(–) showing that current inhibition followed a single exponential decay with the indicated time constant (bottom graph, red line). **E.** Same as D with a test potential to 0 mV. **F.** Inhibition time constants of wash-in from Kv7.2 current measured as shown in D and E. Like with XE991, time constants decreased with depolarizing potentials. ** < 0.01, non-parametric ANOVA (Kruskal-Wallis test) followed by Mann–Whitney test, n = 5. Error bars show SEM.

Figure 7. Linopirdine interaction kinetics with Kv7.2 channels in relation to membrane potential. A. Representative current traces showing Kv7.2 current recovery after washout of 30 μM linopirdine from cells held at -30 mV or -70 mV. For -30 mV holding potential during washout, Kv7.2 currents were monitored by 1-second step hyperpolarizations to -60 mV. For -70 mV holding potential, cells received a 200-ms step depolarization to 0 mV. **B.** Summary showing almost full recovery of Kv7.2 current when cells were washed at -30 mV, while showing slow and limited recovery at -70 mV. **C.** Similar full recovery was observed with heteromeric Kv7.2/3 channels at -30 mV. **D.** Current recovery during washout from 30 μM linopirdine at indicated holding potentials. T = 0 indicates beginning of washout. Current was measured by 500-ms step hyperpolarization to -60 mV with 20 second intervals from indicated holding potentials. **E.** Summary of current recovery time constants at indicated holding potentials during washout. ** <0.01, non-parametric ANOVA (Kruskal-Wallis test) followed by Mann–Whitney test, n = 5. Error bars show SEM.

Figure 8. XE991 and linopirdine interaction with Kv7.2 relates with activation of single subunit. A. Activation curve for Kv7.2 channel (blue curve, Ch_a), and one-quarter power of its Boltzmann function (orange curve, $Ch_a^{1/4}$). Activation curve for a single subunit (red curve, Sub_a) and its fourth power function (purple curve, Sub_a^4) are also shown (see text for details). **B.** Relative inhibition time constants calculated from Fig. 4C (XE991, open circle) and Fig. 7C (linopirdine, orange circle) normalized to those from 0 mV plotted as a function of voltage. The reciprocal of the activation curves of Ch_a, $Ch_a^{1/4}$ and Sub_a shown in panel A are also shown. **C.** Relative recovery time constants from experiments shown in Fig. 4 & 5B (XE991, open triangle) and Fig. 6E & 7E (linopirdine, orange triangle), overlaid with the reciprocal of the activation curves of Ch_a, $Ch_a^{1/4}$ and Sub_a. **D.** Schematic model for interaction between linopirdine and

Kv7.2 channel. **E.** Schematic model for interaction between XE991 and Kv7.2 channel. Error bars show SEM.

JPET Fast Forward. Published on May 8, 2017 as DOI: 10.1124/jpet.117.241679
This article has not been copyedited and formatted. The final version may differ from this version.

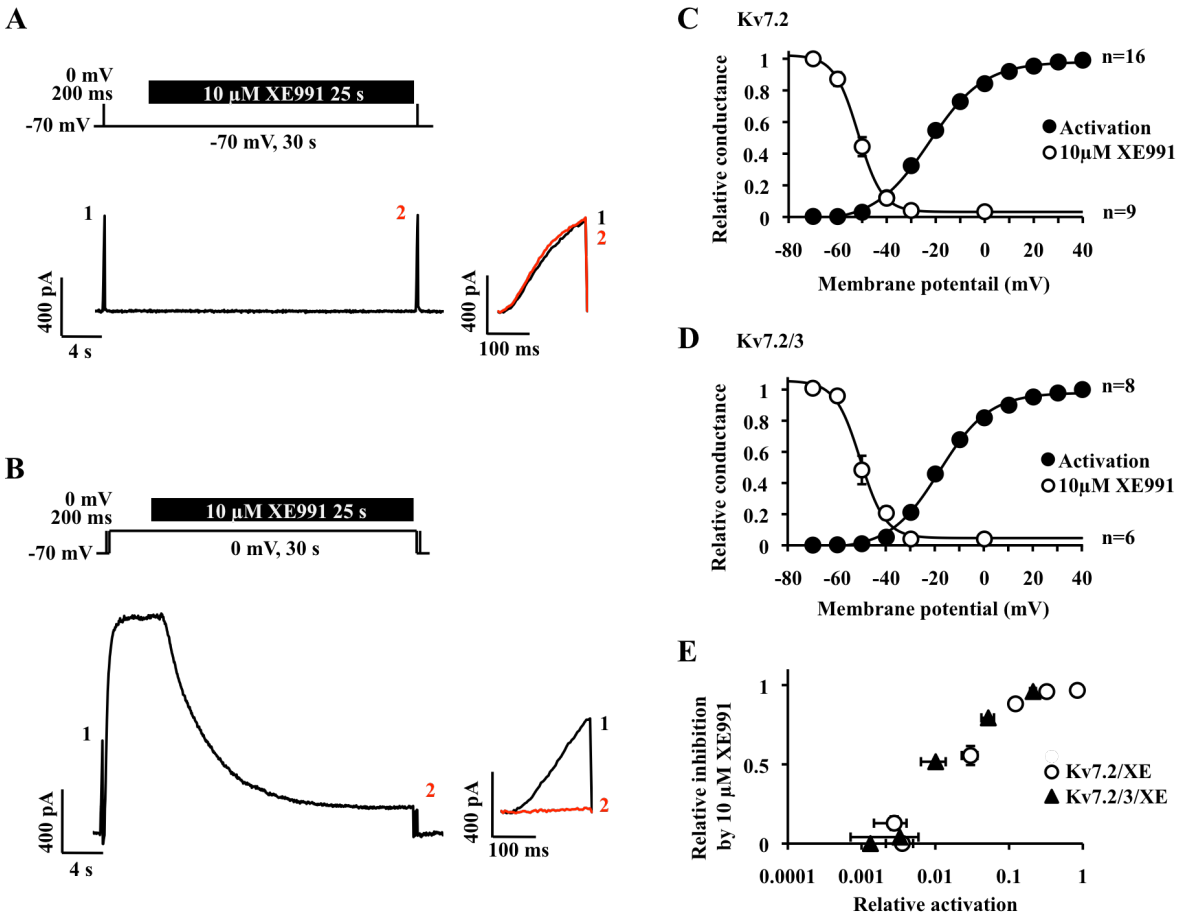

Figure 1

JPET Fast Forward. Published on May 8, 2017 as DOI: 10.1124/jpet.117.241679
This article has not been copyedited and formatted. The final version may differ from this version.

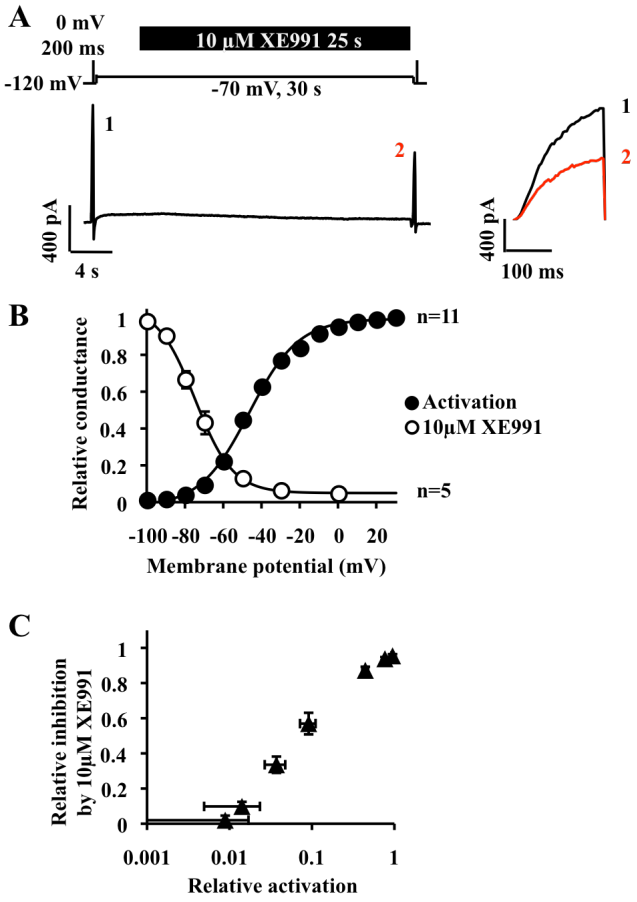

Figure 2

JPET Fast Forward. Published on May 8, 2017 as DOI: 10.1124/jpet.117.241679
This article has not been copyedited and formatted. The final version may differ from this version.

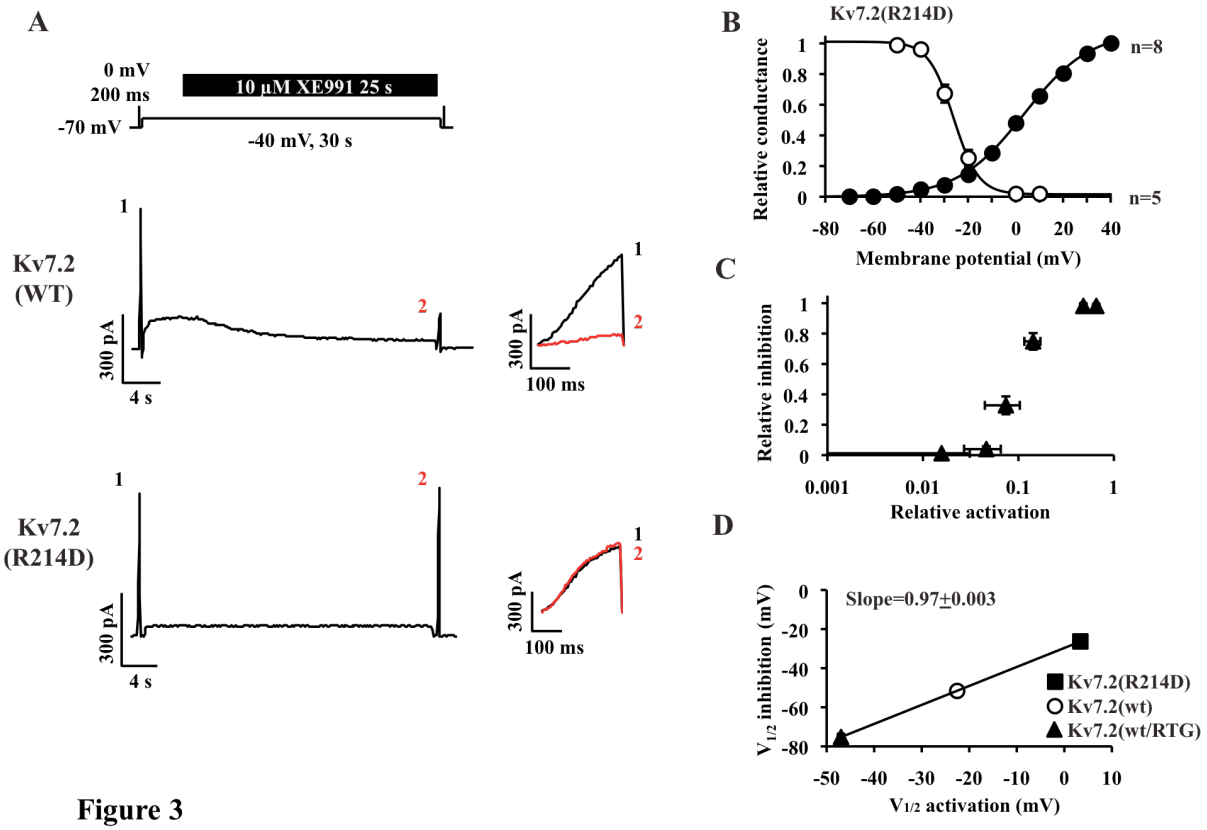

Figure 3

JPET Fast Forward. Published on May 8, 2017 as DOI: 10.1124/jpet.117.241679
This article has not been copyedited and formatted. The final version may differ from this version.

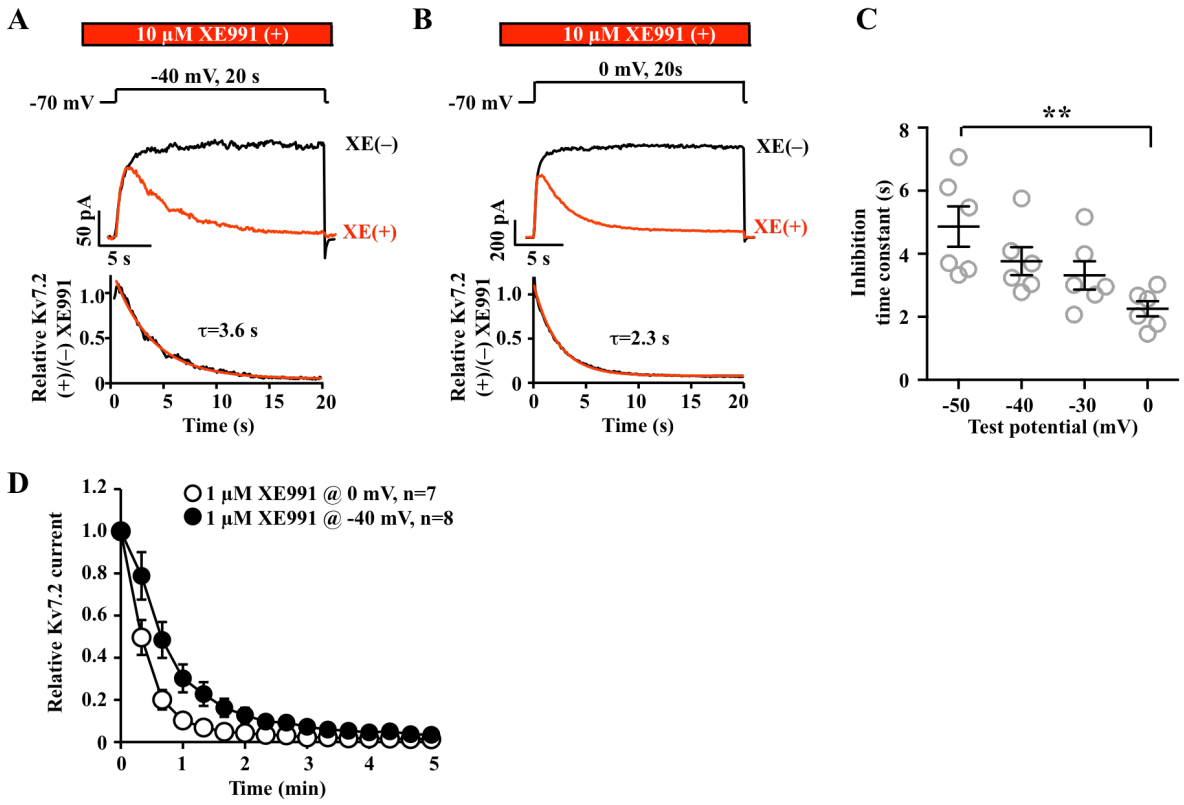

Figure 4

JPET Fast Forward. Published on May 8, 2017 as DOI: 10.1124/jpet.117.241679
This article has not been copyedited and formatted. The final version may differ from this version.

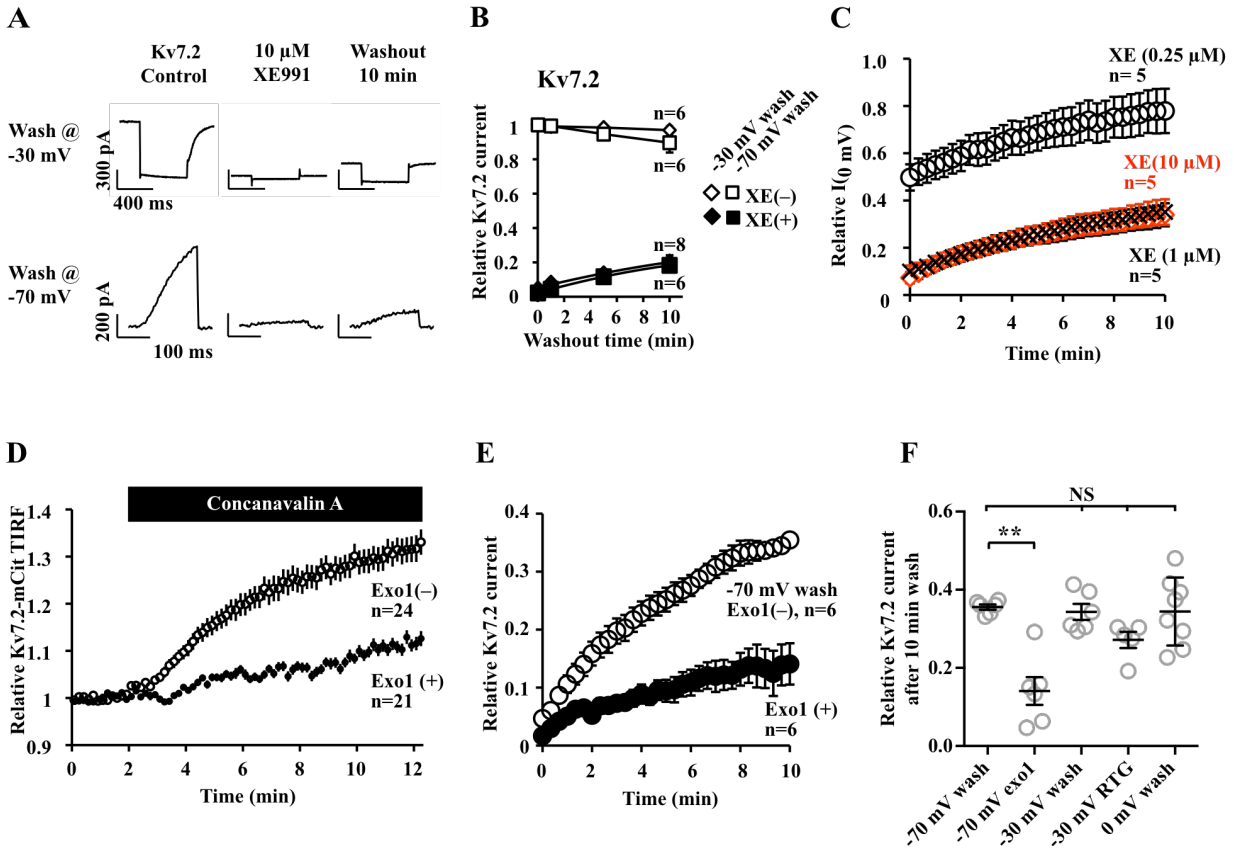

Figure 5

JPET Fast Forward. Published on May 8, 2017 as DOI: 10.1124/jpet.117.241679
This article has not been copyedited and formatted. The final version may differ from this version.

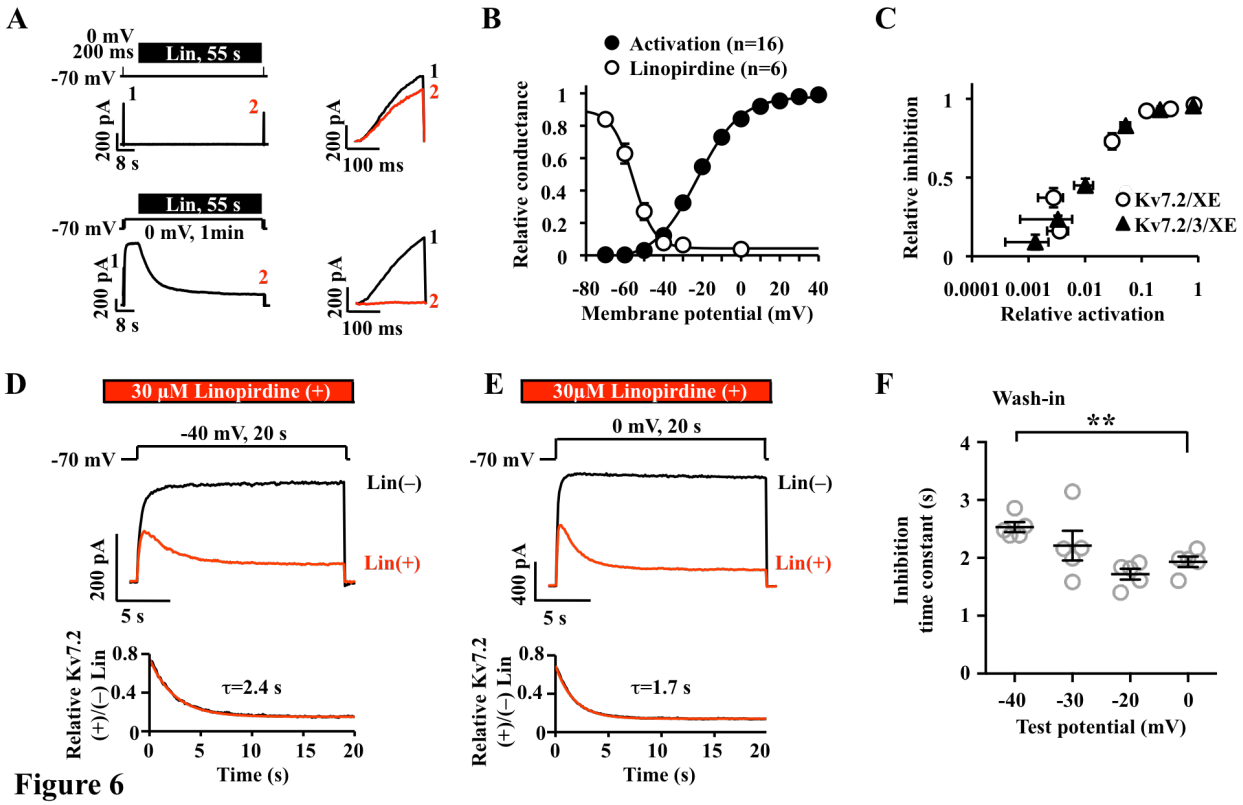

Figure 6

JPET Fast Forward. Published on May 8, 2017 as DOI: 10.1124/jpet.117.241679
This article has not been copyedited and formatted. The final version may differ from this version.

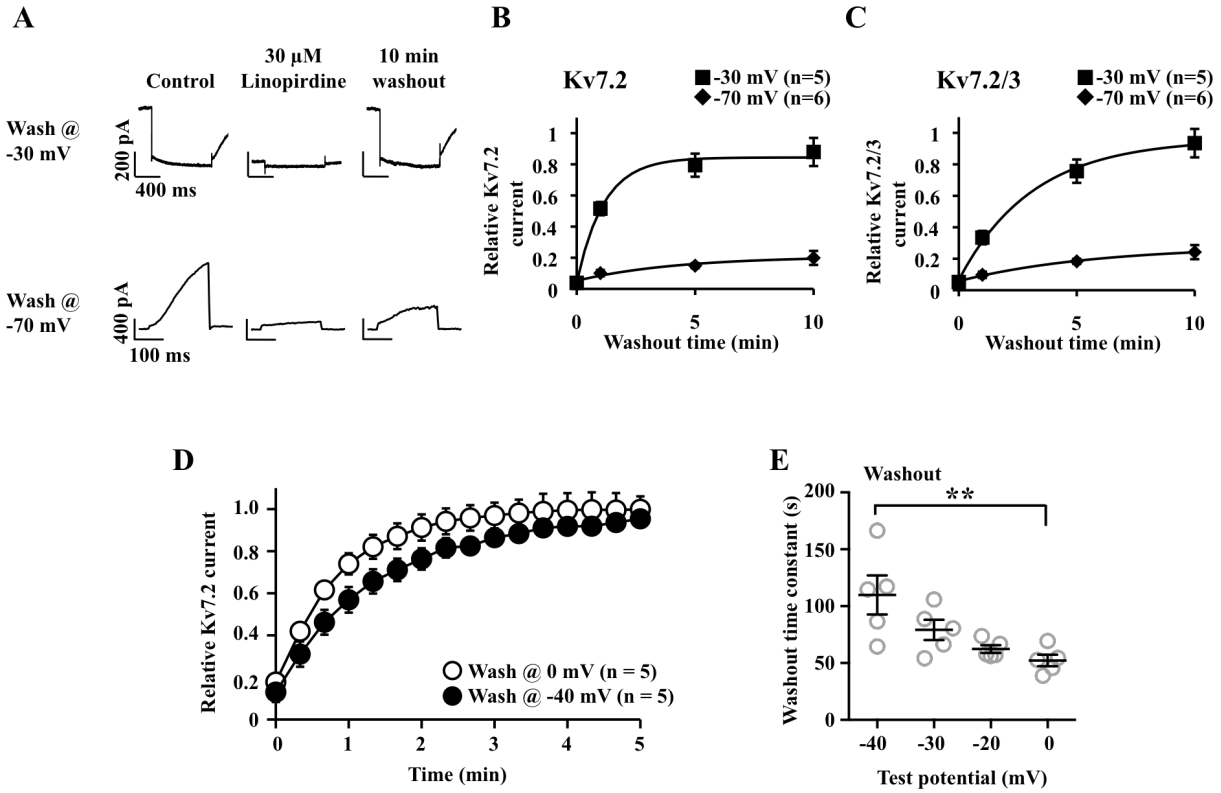

Figure 7

JPET Fast Forward. Published on May 8, 2017 as DOI: 10.1124/jpet.117.241679
This article has not been copyedited and formatted. The final version may differ from this version.

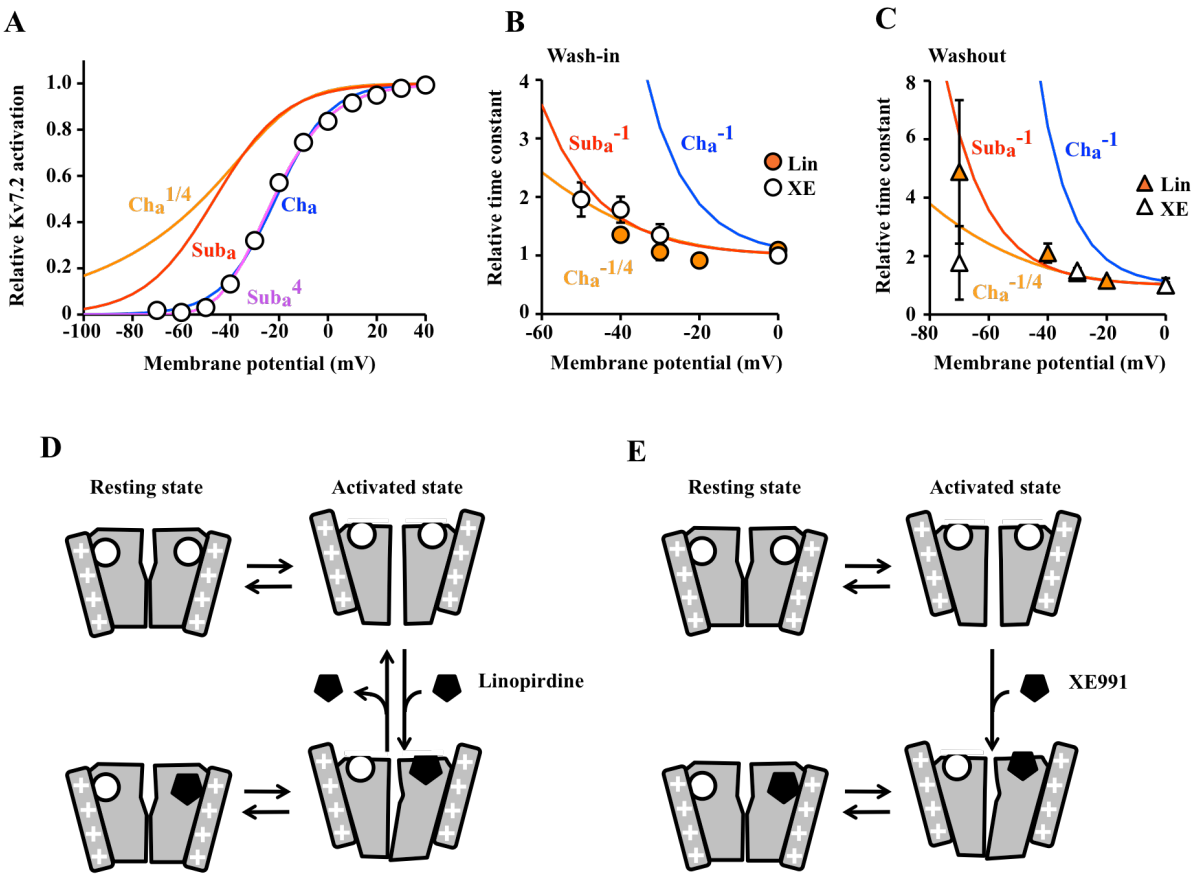

Figure 8

Supplemental data

XE991 and Linopirdine are state-dependent inhibitors for Kv7/KCNQ channels that favor activated single subunits.

Derek L Greene, Seungwoo Kang, and Naoto Hoshi

Journal of Pharmacology and Experimental Therapeutics

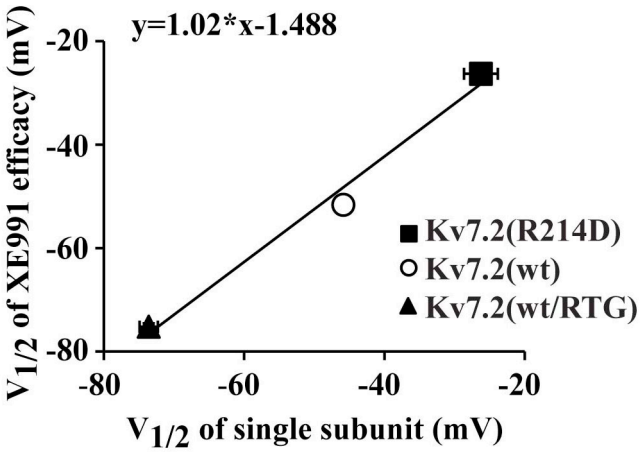

Supplementary Figure 1. Relationships between $V_{1/2}$ of XE991 efficacy and single subunit activation. Pooled results from Fig. 3D re-plotted for single subunit activation. $V_{1/2}$ of subunit activation showed almost complete match to that of XE efficacy in all three conditions. Best-fit linear regression equation is shown. Error bars show SEM.